Higher-Resolution MR Elastography Reveals Early Mechanical Signatures of Neuroinflammation in Patients with Clinically Isolated Syndrome

Andreas Fehlner, Diplomphysiker,[1] Janina Ruth Behrens, Physician,[2,3] Kaspar-Josche Streitberger, MD,[1,2] Sebastian Papazoglou, PhD,[3] Jürgen Braun, PhD,[4] Judith Bellmann-Strobl, MD,[3,5,7] Klemens Ruprecht, MD,[2,5] Friedemann Paul, MD,[3,5,7] Jens Würfel, MD,[3,6] and Ingolf Sack, PhD[1]*

Purpose: To assess if higher-resolution magnetic resonance elastography (MRE) is a technique that can measure the in vivo mechanical properties of brain tissue and is sensitive to early signatures of brain tissue degradation in patients with clinically isolated syndrome (CIS).

Materials and Methods: Seventeen patients with CIS and 33 controls were investigated by MRE with a 3T MRI scanner. Full-wave field data were acquired at seven drive frequencies from 30 to 60 Hz. The spatially resolved higher-resolution maps of magnitude $|G^*|$ and phase angle φ of the complex-valued shear modulus were obtained in addition to springpot model parameters. These parameters were spatially averaged in white matter (WM) and whole-brain regions and correlated with clinical and radiological parameters.

Results: Spatially resolved MRE revealed that CIS reduced WM viscoelasticity, independent of imaging markers of multiple sclerosis and clinical scores. $|G^*|$ was reduced by 14% in CIS (1.4 ± 0.2 kPa vs. 1.7 ± 0.2 kPa, $P < 0.001$, 95% confidence interval [CI] [–0.4, –0.1] kPa), while φ (0.66 ± 0.04 vs. 0.67 ± 0.04, $P = 0.65$, 95% CI [–0.04, 0.02]) remained unaltered. Springpot-based shear elasticity showed only a trend of CIS-related reduction (3.4 ± 0.5 kPa vs. 3.7 ± 0.5 kPa, $P = 0.06$, 95% CI [–0.6, 0.02] kPa) in the whole brain.

Conclusion: We demonstrate that CIS leads to significantly reduced elasticity of brain parenchyma, raising the prospect of using MRE as an imaging marker for subtle and diffuse tissue damage in neuroinflammatory diseases.

J. MAGN. RESON. IMAGING 2016;44:51–58.

Clinically isolated syndrome (CIS) is considered the first clinical manifestation of an inflammatory demyelinating disorder of the central nervous system (CNS), which may later become multiple sclerosis (MS).[1] CIS is defined as a first episode of neurological symptoms with features suggestive of MS that lasts at least 24 hours in the absence of fever, infection, or encephalopathy.[1,2] Commonly affected brain regions include the optic nerve, spinal cord, brainstem, cerebellum, and the cerebral hemispheres.[1] Conversion to MS is seen in ~60% of all cases.[3] The prediction of MS based on clinical and paraclinical markers in CIS is an active area of research.[3–6] Thus, the evaluation of patients at the very onset of MS may provide new insights into the mechanisms leading to axonal loss and neuronal dysfunction, which occur early in the disease course.[7,8]

View this article online at wileyonlinelibrary.com. DOI: 10.1002/jmri.25129

Received Jun 17, 2015, Accepted for publication Dec 1, 2015.

The first two and last two authors contributed equally to this work.

*Address reprint requests to: I.S., Department of Radiology, Charité – Universitätsmedizin Berlin, Charitéplatz 1, 10117 Berlin, Germany. E-mail: ingolf.sack@charite.de

From the [1]Department of Radiology, Charité – Universitätsmedizin Berlin, Berlin, Germany; [2]Department of Neurology, Charité – Universitätsmedizin Berlin, Berlin, Germany; [3]NeuroCure Clinical Research Center, Charité – Universitätsmedizin Berlin, Berlin, Germany; [4]Institute of Medical Informatics, Charité – Universitätsmedizin Berlin, Berlin, Germany; [5]Clinical and Experimental Multiple Sclerosis Research Center, Department of Neurology, Charité – Universitätsmedizin Berlin, Berlin, Germany; [6]Medical Image Analysis Center Basel, Switzerland; and [7]Experimental and Clinical Research Center, Charité – Universitätsmedizin Berlin, Max Delbrück Center for Molecular Medicine in the Helmholtz Association, Berlin, Germany.

Magnetic resonance elastography (MRE) measures the mechanical consistency of brain tissue in a noninvasive, image-resolved way.[9–11] Previous studies have revealed that MS causes brain softening.[12,13] Preclinical MRE findings in mouse models of MS[14,15] suggest that this decrease of elasticity is most likely an effect of disseminated neuroinflammation and demyelination. In patients, different subtypes of MS have been investigated by MRE. In patients with a relapsing-remitting course of the disease (RRMS), a marked decrease in shear modulus was observed, while brain viscosity remained unaltered.[12] Primary and secondary progressive MS (PPMS, SPMS) were found to be associated with a more marked shear modulus reduction and a concomitant decrease in brain viscosity.[13]

Previous work was based on a method of multifrequency MRE in which both shear elasticity and shear viscosity of the whole central brain parenchyma were obtained without higher spatial resolution.[9] Recent technical advances in cerebral MRE have improved the spatial resolution of the so-called elastograms by introducing multifrequency inversion and full 3D wave fields acquired at several frequencies.[16–18] This method of higher-resolution multifrequency MRE (in the following denoted as MMRE) is used to identify signatures of neuroinflammation at the very onset of MS. The current study complements previous investigations by springpot-based viscoelasticity MRE (in the following denoted as VMRE) showing gradual mechanical degradation of brain tissue in patients with MS.[12,13]

The purpose of this study was to apply MMRE for the detection of early signatures of brain tissue degradation in patients with CIS and to analyze the gradual mechanical degradation of brain tissue associated with MS by VMRE.

Materials and Methods

Subjects

The Berlin CIS cohort (NCT01371071) is an ongoing prospective observational study of patients with a first clinical event suggestive of inflammatory demyelination or with early RRMS, which started recruitment in January 2011. Inclusion criteria were: age >18 years and a first clinical event suggestive of CNS demyelination.[19]

Seventeen CIS patients (mean age 30.4 years, range 22–47 years, 7 females) participated in this substudy. Four of them were recently included with a relatively short observational time (<1 year). The clinical course of 13 was observed for at least 1 year. After 1 year, five patients developed MS, eight remained CIS. After 2 years, two more patients developed MS so that seven patients in total were MS-transformers. Correspondingly, two groups of patients were further compared (MS-subgroup, age: 26.3 ± 3.7 years vs. CIS-subgroup, 35.2 ± 6.3 years).

A group of 33 healthy controls (HC; mean age 31.5 years, range 18–53 years, 15 females) was investigated for comparison. CIS and HC groups were matched for age ($P = 0.66$) and gender ($P = 0.78$).

The neurological examination and the evaluation of the degree of neurologic impairment with the Expanded Disability Status Scale EDSS[20] were performed at the date of the MMRE measurements. The study was approved by the Ethics Committee of the Charité – Universitätsmedizin Berlin in conformity with the Declaration of Helsinki. All study participants gave informed written consent prior to the examination.

Imaging Protocol

All experiments were performed at the Berlin Center of Advanced Neuroimaging on a 3T whole-body MRI (Magnetom Trio; Siemens Healthcare, Erlangen, Germany), using a 12-channel head coil. For anatomical T_1-weighted imaging with acquisition of high-resolution isotropic 3D whole-brain datasets (1 mm^3), a magnetization-prepared rapid acquisition of gradient echoes (MPRAGE; time to echo [TE] 3.03 msec, repetition time [TR] 1900 msec, inversion time [TI] 900 msec, flip angle 9°) was applied. For T_2-weighted imaging, a single-slab 3D T_2-weighted turbo-spin-echo (TSE) sequence with high sampling efficiency (SPACE) was selected without (T_2w; TE 388 msec, TR 6000 msec, echo train length [ETL] 848 msec) or with fluid attenuation inversion recovery pulse (FLAIR; TE 502 msec, TR 5000 msec, TI 2100 msec, ETL 972 msec). To exclude brainstem and infratentorial artifacts, an axial double-echo proton density / T_2-weighted sequence was added (TE 14/87 msec, TR 3400 msec, flip angle 120°, voxel resolution 1 × 1 × 3 mm^3, no gap). Contrast-enhanced images were acquired with a volumetric interpolated brain imaging sequence optimized for short acquisition time with asymmetric *k*-space sampling and interpolation (VIBE; 1 mm^3, TE 2.2 msec, TR 4.85 msec, flip 9°) 8 minutes after body-weight-adapted 0.1 mmol/kg contrast medium injection (Gadovist, 1 mmol/ml gadobutrol; Bayer Austria, Wien). T_2w lesion count and lesion volume were calculated using the OsiriX software toolbox (OsiriX Foundation, Geneva, Switzerland) and in-house applications based on the SPACE 3D T_2 sequence.

Mechanical Wave Excitation and MMRE

A nonmagnetic vibration generator was placed at the end of the patient table and connected to a head cradle inside the head coil.[17] The piezoelectric ceramics (18 cm length, 2 cm diameter) of the driver was fed by a 150 V alternating current. The analog power amplifier was capable of recharging the high capacitance of the ceramics of 63 μF at 100 Hz vibration frequency. A waveform generator was integrated in the amplifier device and customized to interpret the duration and sequence of incoming Transistor–Transistor Logic (TTL) trigger pulses for the timing and the waveform of the outgoing vibration signals. This so-called smart trigger was used to automatically switch the frequency of the mechanical vibration by the sequence protocol of the MRI scanner. The vibration was initiated at least 100 msec before the start of the motion-encoding gradients (MEG) to allow the wave traveling into the brain. Seven harmonic drive frequencies from 30 to 60 Hz in 5-Hz increments were applied in consecutive MRE scans.

Full 3D wave fields in 15 contiguous image slices of 1.9 × 1.9 × 1.9 mm^3 resolution were acquired using a single-shot spin-echo echo-planar imaging sequence with trapezoidal flow-compensated MEG. The MEG was applied along all three axes of the scanner coordinate system in consecutive scans.[21] In the following, further

imaging parameters are summarized: TR 2980 msec; TE 71 msec; field of view (FoV) 190 × 160 mm^2; matrix size 100 × 84; MEG frequencies (number of cycles): 37 (1), 37 (1), 37 (2), 37 (2), 41 (1), 45 (1) Hz corresponding to 30, 35, 40, 45, 50, 55, 60 Hz vibration frequency, respectively (note: MEG frequency and cycle number were chosen to achieve highest encoding efficiency according to the principle of fractional motion encoding[22]; MEG amplitude: 35 mT/m; 8 dynamic scans at equally spaced timepoints during a full wave cycle, ~1 minute scan time for each frequency, resulting in a total acquisition time of ~7 minutes for a full MMRE dataset consisting of 2520 images.

Data Postprocessing

HIGHER-RESOLUTION MMRE. MMRE data processing was identical to the method recently outlined.[23] The following steps were performed from raw phase data to high-resolution elastograms: 1) Gradient unwrapping[24] after 2D Gaussian denoising with 5 pixel kernel edge size and $\sigma = 0.65$. 2) Temporal Fourier transformation to produce six complex-valued wave derivative (strain) images for each harmonic drive frequency (two in-plane derivatives in each field component). 3) Noise suppression by a 2D Butterworth lowpass filter with a threshold of 100 m^{-1}. 4) Multifrequency dual elasto visco (MDEV) inversion as detailed previously.[18,23,25]

MDEV inversion provides two independent mechanical constants, $|G^*|$ and φ, corresponding to the magnitude and phase of complex shear modulus G^*, respectively. $|G^*|$ is the proportionality between peak stress and resulting strain, while φ is the phase angle by which a harmonic oscillation in a viscous medium lags behind the same oscillation in a lossless medium.[26] It is well known that both parameters vary with excitation frequency.[9] In MDEV inversion this information is sacrificed for higher-resolution parameter mapping. Instead, $|G^*|$ and φ refer to an effective harmonic frequency given by the mean of all vibration frequencies and weighted by the corresponding wave amplitudes.

VISCOELASTICITY-RESOLVED MRE BASED ON THE SPRINGPOT MODEL (VMRE). For validation and comparison to the literature, we used standard direct inversion of the complex-valued 2D Helmholtz equation[27] performed at each single drive frequency, followed by springpot-model fitting of the dispersion function of complex shear modulus G^*. This method, as detailed in Ref. 13, involves the following steps: 1) 2D unwrapping of phase images using Flynn's algorithm.[28] 2) Temporal Fourier transformation in order to select $u_j^*(\omega_l)$, the complex-valued wave images at angular drive frequency ω_l ($j = 1,2$ [slice-select and phase-encode wave field components] and $l = 1..8$). 3) Bandpass filtering with filter thresholds given in Ref. 13 and interpolated to the frequencies of our current study: 6.7 (55.9), 7.8 (62.8), 8.8 (71.1), 9.6 (81.9), 10 (90.9), 10 (96), 10 (99.5) m^{-1} at 30, 35, 40, 45, 50, 55, and 60 Hz, respectively (upper threshold in parentheses). 4) Direct inversion by the equation:

$$G^*(\omega_l) = -\rho\omega_l^2 \frac{1}{2} \sum_{j=1}^{2} \frac{u_j^*(\omega_l)}{\Delta u_j^*(\omega_l)} \quad (1)$$

where Δ denotes the 2D Laplacian and ρ the material's density of 1000 kg/m^3. 5) Averaging of $G^*(\omega_l)$ within the entire parenchyma visible in the examined brain region, followed by a springpot fit of spatially averaged $G^*(\omega_l)$-values by:

$$G^*_{\text{springpot}}(\omega_l) = \kappa(i\omega_l)^\alpha \text{ with } \kappa = \mu^{1-\alpha}\eta^\alpha \quad (2)$$

where μ and α represent frequency independent fit variables and η is the specific viscosity of brain tissue of = 3.7 Pa·s.[29]

BRAIN VOLUME SEGMENTATION. Global gray matter atrophy was assessed in all subjects based on T_1-weighted MRI scans using SIENAX as implemented in FSL 5.0.6 (FMRIB Software Library, Oxford, UK). Before segmentation, 3D images were coregistered to the 1 mm MNI standard space template using a rigid body registration with 6 degrees of freedom. After coregistration the MRI scans were corrected for intensity nonuniformity using the N3 algorithm supplied with Mipav 5.4.2 (Center for Information Technology, National Institutes of Health, Bethesda, MD). Gray matter (GM), white matter (WM), and full brain volumes normalized with respect to the standard space brain size were used for further statistical analysis. In line with previous findings, we considered that brain volumes of patients at this early disease phase (CIS) were equal to those of the HC group or that edematous inflammatory processes might possibly lead to an overestimation of full brain volume compared to HC.[19,30]

NORMALIZATION OF MMRE MAPS. Four representative slices in each subject were manually selected based on their anatomical compliance in the MRE magnitude images. Next, normalized templates were created using the Advanced Normalization Tools (ANTS).[31] Each MMRE map was then registered and transformed to the template space by the individual deformation map and affine matrix. For this purpose, cross-correlation was applied as similarity metric, and the symmetric normalization transformation model was used for diffeomorphic image registration. Finally, the normalized maps were averaged within each group to generate group mean MMRE maps.

Statistical Analysis

We evaluated tissue viscoelasticity in the WM region for the full brain obtained by the segmentation toolbox of SPM12 similar to the WM regions proposed in Ref. 17. Additionally, we used a full brain mask (entire parenchyma including cerebrospinal fluid [CSF] in small sulci, excluding ventricles and large CSF-filled sulci).

Statistical analysis was performed using the MatLab Statistics Toolbox (MathWorks, Natick, MA) and SPSS statistics v. 23 (IBM, Armonk, NY). The results were tabulated as arithmetic mean ± standard deviation. Differences between patients and controls were tested by a two-tailed Student's t-test. Differences between the two patient subgroups were tested by a Wilcoxon rank-sum test. Here, normal distribution was not assumed due to the limited number of subjects. $P < 0.05$ was considered significant for all tests. For the assessment of the relationship between MRE and time to MS conversion (Cox regression (survival) analysis) SPSS was used.

Results

MMRE

Figure 1 shows four representative slices of group-averaged parameters $|G^*|$ and φ along with difference maps $\Delta|G^*|$ and $\Delta\varphi$, representing the relative change in viscoelasticity in

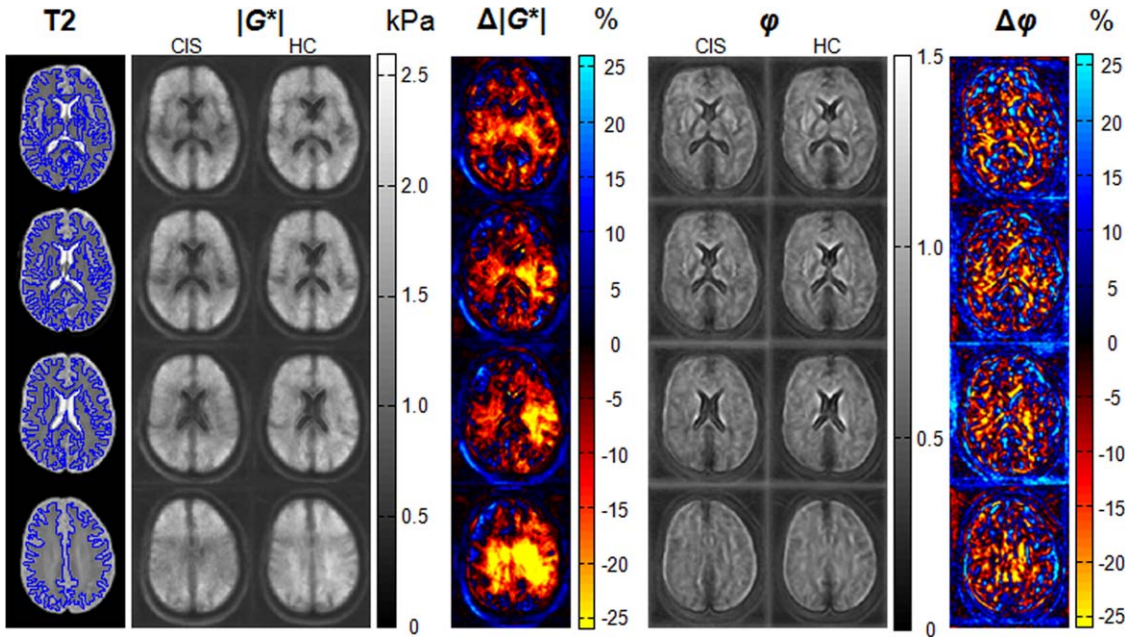

FIGURE 1: Viscoelasticity changes in brain tissue due to CIS: While the magnitude modulus $|G^*|$ clearly decreases from patients to healthy controls (HC) (best represented by the relative ratio maps $\Delta|G^*|$), the phase angle φ is not sensitive to CIS. The maps illustrate group-averaged values normalized to a standard brain. For visualization, a subgroup of the control group was chosen in order to have the same number of patients and controls.

CIS patients versus HC. It is clearly visible that both storage and loss moduli are reduced in patients, causing lower $|G^*|$ values while φ remains unchanged. The disseminated reduction of $|G^*|$ is pronounced in WM. Figure 2a compares MMRE parameters averaged in WM between groups ($|G^*|$: 1652 ± 232 Pa vs. 1414 ± 201 Pa, 95% CI [104, 371] Pa; φ: 0.67 ± 0.05 vs. 0.66 ± 0.05, $P = 0.65$, 95% CI [–0.02, 0.04]), demonstrating a significant CIS-related decrease in $|G^*|$ (~14%, $P < 0.001$). The analysis of averaging the elastograms over the whole brain (excluding ventricles and large CSF-filled sulci) shows also a decrease of 10% with $P < 0.01$ ($|G^*|$: 1470 ± 176 Pa vs. 1319 ± 159 Pa, 95% CI [48, 253] Pa; φ: 0.61 ± 0.04 vs. 0.62 ± 0.04, 95% CI [–0.03, 0.02]). MMRE parameters were not different in patients who developed MS as compared to patients who remained CIS (CIS: $|G^*|$: 1260 ± 123 Pa vs. MS: 1346 ± 190 Pa, $P = 0.34$, and CIS: φ: 0.61 ± 0.04 vs. MS: 0.63 ± 0.03 Pa, $P = 0.53$ in whole brain; CIS: $|G^*|$: 1343 ± 141 Pa vs. MS: 1444 ± 256 Pa,

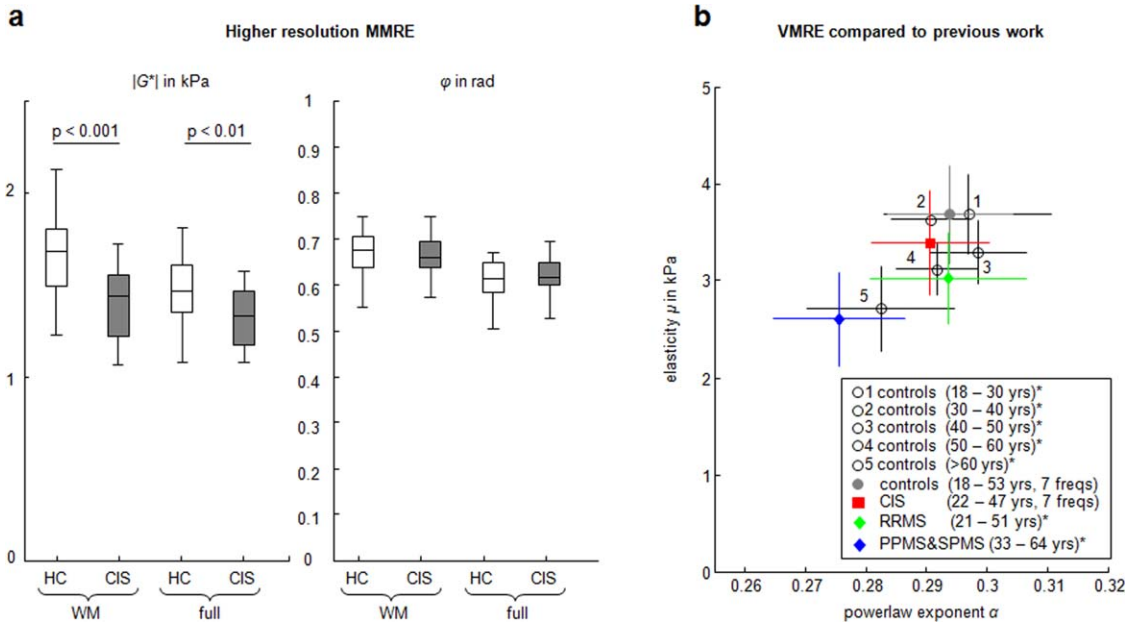

FIGURE 2: Group-averaged MMRE parameters of WM according to the higher-resolution processing pipeline based on MDEV inversion (left) and conventional springpot fitting of modulus values obtained by Helmholtz inversion on the right. *Data taken from Ref. 32.

$P = 0.40$ and CIS: φ: 0.66 ± 0.04 vs. MS: 0.67 ± 0.05 Pa, $P = 0.78$ in WM).

VMRE

The springpot parameter μ measured by VMRE tended to be lower in patients (HC: 3685 ± 503 Pa vs. CIS: 3390 ± 541 Pa, $P = 0.06$, 95% CI [–15, 604] Pa). While not statistically significant, this reduction is consistent with the previously observed decrement of μ (Fig. 2b).[32] The powerlaw exponent α was unaltered (HC: 0.294 ± 0.010 vs. CIS: 0.291 ± 0.010, $P = 0.30$, 95% CI [–0.003, 0.009]). The Pearson correlation coefficient of μ to $|G^*|$ of the full brain is 0.72 for CIS patients and 0.62 for healthy controls ($P < 0.01$). No significant correlation was found between the powerlaw exponents α and φ ($P > 0.19$).

Volumetry

Brain volumes were similar in both groups (HC vs. CIS: full brain: 1.58 ± 0.07 dm^3 vs. 1.58 ± 0.06 dm^3, $P = 0.80$, 95% CI [–0.05, 0.04] dm^3); GM: 0.83 ± 0.05 dm^3 vs. 0.82 ± 0.03 dm^3, $P = 0.33$, 95% CI [–0.01, 0.04] dm^3; WM: 0.74 ± 0.03 dm^3 vs. 0.76 ± 0.03 dm^3, $P = 0.06$, 95% CI [–0.04, $+0.05 \cdot 10^{-2}$] dm^3).

Clinical and Radiological Parameters

MRE was neither correlated with the time from CIS diagnosis to the onset of MS (Cox-regression $P \geq 0.16$) nor with the number of relapses (1 year after CIS diagnosis, $n = 13$, $|r| \leq 0.35$, $P \geq 0.24$; 2 years after diagnosis, $N = 7$, $r \leq 0.69$, $P \geq 0.09$). Similarly, MRE was not correlated with disease duration (time from diagnosis to MRE exam, $r \leq 0.36$, $P \geq 0.16$), with time from last clinical relapse to MRE exam ($|r| \leq 0.30$, $P \geq 0.24$), nor with EDSS (median EDSS = 1.5, range: 0–3, $|r| \leq 0.27$, $P \geq 0.29$).

Only one patient had a contrast-enhancing lesion. The median number of T_2w lesions was 3 (range: 0–56) without correlation to MRE ($r \leq 0.30$, $P \geq 0.23$). T_2 lesion volume was 0.62 ± 0.91 cm^3 (range: 0–3.21 cm^3) also without correlation to MRE parameters ($r \leq 0.35$, $P \geq 0.17$).

Discussion

We studied WM viscoelasticity in the earliest stages of MS. Compared to the pronounced decrease in shear elasticity observed in patients with more advanced MS,[12,13] the effect observed in the current study is weak, as there was only a trend in μ. Nevertheless, using advanced methods for higher-resolution mechanical imaging such as MDEV-inversion-based MMRE allows us to delineate the brain regions in which viscoelasticity has been altered in response to autoimmune CNS inflammation before the manifestation of MS and in the absence of overt brain atrophy, which may occur in early MS.[33,34]

In the past decade, MRI has improved early MS diagnosis by demonstrating spatiotemporal lesion dissemination. Notwithstanding this success, conventional MR parameters only moderately correlate with clinical disability—a phenomenon termed the "clinico-radiological paradox."[35] Consequently, the known correlation between clinical and pathological phenotype is still limited.

Unlike conventional imaging markers, viscoelastic properties can reveal structural alterations in biological tissues at multiple scales with high sensitivity.[13] For this reason, MRE was recently found to detect a decrease of whole-brain viscoelasticity in patients with RRMS compared to matched healthy volunteers, indicating a widespread degradation of tissue integrity going beyond the few T_2 lesions revealed by conventional MRI.[12] Schregel et al.[15] demonstrated in a cuprizone mouse model of MS that the magnitude of the complex shear modulus decreases with both progressive demyelination and alterations of the structural integrity of the extracellular matrix (ECM). This work was confirmed by an MRE study in a model of experimental autoimmune encephalomyelitis (EAE) demonstrating a clear correlation between viscoelastic tissue alteration and the magnitude of perivascular T-cell infiltration.[14] Both in vivo MRE studies in mouse models of MS shed light on the high sensitivity of MRE to structural ECM alterations and immune cell infiltration in EAE.

This sensitivity is enhanced by MDEV inversion-based cerebral MRE, revealing details of brain anatomy by a pixel-wise resolution,[17,18,23,25] which clearly outperforms the resolution of single-frequency Helmholtz inversion.[9] Conventional direct inversion relies on filter banks capable of extracting components of propagating shear waves from the reverberant patterns of intracranial waves. Standing waves would ultimately cause wave nodes (regions without elastic deformation) in which elastographic parameters cannot be recovered. Our multifrequency inversion approach accounts for amplitude nulls and noise by averaging the magnitude displacements (and the magnitude Laplacians) in each voxel over all components and drive frequencies, thereby providing better-conditioned wave patterns for inversion. As a limitation, MDEV inversion yields lower $|G^*|$ values than predicted by springpot fitting and single-frequency-based MRE,[9,36–38] which is—as discussed in Ref. 17—a result of low vibration frequencies (e.g., 30 Hz incorporated in our inversion), non-Gaussian noise, and preserved wave scattering due to weak lowpass filter capacities. Despite the limited comparability between $|G^*|$ and μ, MDEV inversion yields consistent values, as seen by comparison of our mean WM value of 1652 ± 232 Pa with values reported in Ref. 17 (1252 ± 260 Pa), which included elderly volunteers, and with values of normal-appearing WM in patients with glioblastoma (1540 ± 270 Pa).[23] We therefore regard MDEV-inversion-based MRE as a stable tool for viscoelastic parameter quantification capable of generating pixel-resolved maps of $|G^*|$ and φ. To further increase the accuracy and clinical potential of cerebral MRE, future research efforts should be invested in the development of reconstruction algorithms for anisotropic[39,40] and

TABLE 1. Demographic Data, Clinical Scores (EDSS, T2 Lesions), Brain Volumes, Viscoelastic Constants μ and α According to the Springpot Model and $|G^*|$ and φ obtained by Higher-Resolution MMRE. Δ refers to the relative change in %.

Group	CIS	HC
N	17	33
Female *N*	7	15
Age in years (mean ± SD; range)	30.41 ± 6.68 ; 22–47	31.52 ± 9.12 ; 18–53
EDSS (median; range)	1.5 ; 0–3	
T2 lesions count (median; range)	3 ; 0–56	
T2 lesions volume in cm^3 (mean + SD; range)	0.62 ± 0.91 ; 0–3.21	
V(whole brain) in dm^3	1.58 ± 0.06	1.58 ± 0.07
ΔV(whole brain)	0%, $P =$ 0.80	
V(WM) in dm^3	0.76 ± 0.03	0.74 ± 0.03
ΔV(WM)	~-2%, $P =$ 0.06	
V(GM) in dm^3	0.82 ± 0.03	0.83 ± 0.05
ΔV(GM)	~2%, $P =$ 0.33	
μ (whole brain) in Pa	3390 ± 541	3685 ± 503
$\Delta\mu$ (whole brain)	~8%, $P =$ 0.06	
α	0.291 ± 0.01	0.294 ± 0.01
$\Delta\alpha$	~1%, $P =$ 0.30	
$\|G^*\|$ (WM) in Pa	1414 ± 201	1652 ± 232
$\Delta\|G^*\|$ (WM)	~14%, $P <$ 0.001	
φ (WM)	0.66 ± 0.05	0.67 ± 0.05
$\Delta\|\varphi\|$ (WM)	~1%, $P =$ 0.65	
$\|G^*\|$ in Pa (whole brain)	1319 ± 159	1470 ± 176
$\Delta\|G^*\|$ (whole brain)	~10%, $P <$ 0.01	
φ (whole brain)	0.62 ± 0.04	0.61 ± 0.04
$\Delta\|\varphi\|$ (whole brain)	~-1%, $P =$ 0.61	

poroelastic[21,38] parameters as well as in efficient drivers such as those which induce intracranial vibrations in a remote way.[25]

Although encouraging, our study has several limitations. First, the low number of patients prevents valid conclusions on the correlation of MRE parameters with clinical scores. This particularly applies to early pathological changes as associated with CIS in which the clinical manifestation of the disease progression is still under investigation. Furthermore, the test–retest reproducibility of MMRE has never been demonstrated in the literature, leaving us with uncertainty about the variation of cerebral MRE parameters in individuals due to head positioning inside the vibration cradle or possible slice positioning artifacts. Accounting for such effects may increase the accuracy of brain MMRE in future studies and better reveal possible interactions between clinical measures in MS and the viscoelastic properties of the brain.

In conclusion, MMRE was used to study the impact of neuroinflammation on brain viscoelastic properties at an early stage of MS. In a group of CIS patients, a significant reduction of WM viscoelasticity parameterized by the magnitude shear modulus $|G^*|$ on the order of 14% compared to healthy controls was observed. Analyzing the data by conventional single-frequency wave inversion and viscoelastic modeling enabled us to directly compare our findings with data from previous work, which used MRE in patients with more advanced MS, suggesting that MS is accompanied by gradual disseminated softening of brain tissue starting at the very onset of the disease. Future studies will focus on the

development of viscoelasticity as a clinical prognostic marker by correlating MMRE with clinical conversion of CIS. In essence, higher-resolution MMRE is a promising tool that may have the potential to support clinical diagnosis, characterize disease activity, and monitor responses to therapy in both neurodegenerative and neuroinflammatory diseases such as MS.

Acknowledgments

The authors thank Susan Pikol and Cynthia Kraut for excellent technical assistance. A.F. acknowledges a scholarship from the Hanns-Seidel-Foundation. I.S. acknowledges support by the German Research Foundation (Sa901/10).

Conflict of Interest

K.R. received research support from Novartis as well as speaking fees and travel grants from Guthy Jackson Charitable Foundation, Bayer Healthcare, Biogen Idec, Merck Serono, Sanofi/Genzyme, Teva, Roche, and Novartis, and is supported by the German ministry of education and research (BMBF/KKNMS, Competence Network Multiple Sclerosis).

References

1. Miller DH, Chard DT, Ciccarelli O. Clinically isolated syndromes. Lancet Neurol 2012;11:157–169.
2. Schumacker GA, Beebe G, Kibler RF, et al. Problems of experimental trials of therapy in multiple sclerosis: report by the Panel on the Evaluation of Experimental Trials of Therapy in Multiple Sclerosis. Ann N Y Acad Sci 1965;122:552–568.
3. Alroughani R, Al Hashel J, Lamdhade S, Ahmed SF. Predictors of conversion to multiple sclerosis in patients with clinical isolated syndrome using the 2010 Revised McDonald Criteria. ISRN Neurol 2012;2012: 792192.
4. Sbardella E, Greco A, Stromillo ML, et al. Isoprostanes in clinically isolated syndrome and early multiple sclerosis as biomarkers of tissue damage and predictors of clinical course. Mult Scler 2013;19:411–417.
5. Dalton CM, Bodini B, Samson RS, et al. Brain lesion location and clinical status 20 years after a diagnosis of clinically isolated syndrome suggestive of multiple sclerosis. Mult Scler 2012;18:322–328.
6. Kalincik T, Guttmann CR, Krasensky J, et al. Multiple sclerosis susceptibility loci do not alter clinical and MRI outcomes in clinically isolated syndrome. Genes Immun 2013;14:244–248.
7. Scheel M, Finke C, Oberwahrenbrock T, et al. Retinal nerve fibre layer thickness correlates with brain white matter damage in multiple sclerosis: a combined optical coherence tomography and diffusion tensor imaging study. Mult Scler 2014;20:1904–1907.
8. Sinnecker T, Mittelstaedt P, Dorr J, et al. Multiple sclerosis lesions and irreversible brain tissue damage: a comparative ultrahigh-field strength magnetic resonance imaging study. Arch Neurol 2012;69: 739–745.
9. Sack I, Beierbach B, Hamhaber U, Klatt D, Braun J. Non-invasive measurement of brain viscoelasticity using magnetic resonance elastography. NMR Biomed 2008;21:265–271.
10. Kruse SA, Rose GH, Glaser KJ, et al. Magnetic resonance elastography of the brain. Neuroimage 2008;39:231–237.
11. Green MA, Bilston LE, Sinkus R. In vivo brain viscoelastic properties measured by magnetic resonance elastography. NMR Biomed 2008; 21:755–764.
12. Wuerfel J, Paul F, Beierbach B, et al. MR-elastography reveals degradation of tissue integrity in multiple sclerosis. Neuroimage 2010;49: 2520–2525.
13. Streitberger KJ, Sack I, Krefting D, et al. Brain viscoelasticity alteration in chronic-progressive multiple sclerosis. PLoS One 2012;7:e29888.
14. Riek K, Millward JM, Hamann I, et al. Magnetic resonance elastography reveals altered brain viscoelasticity in experimental autoimmune encephalomyelitis. NeuroImage Clin 2012;1:81–90.
15. Schregel K, Wuerfel E, Garteiser P, et al. Demyelination reduces brain parenchymal stiffness quantified in vivo by magnetic resonance elastography. Proc Natl Acad Sci U S A 2012;109:6650–6655.
16. Papazoglou S, Hirsch S, Braun J, Sack I. Multifrequency inversion in magnetic resonance elastography. Phys Med Biol 2012;57:2329–2346.
17. Guo J, Hirsch S, Fehlner A, et al. Towards an elastographic atlas of brain anatomy. PLoS One 2013;8:e71807.
18. Braun J, Guo J, Lützkendorf R, et al. High-resolution mechanical imaging of the human brain by three-dimensional multifrequency magnetic resonance elastography at 7T. Neuroimage 2014;90:308–314.
19. Paolillo A, Piattella MC, Pantano P, et al. The relationship between inflammation and atrophy in clinically isolated syndromes suggestive of multiple sclerosis: a monthly MRI study after triple-dose gadolinium-DTPA. J Neurol 2004;251:432–439.
20. Kurtzke JF. Rating neurologic impairment in multiple sclerosis: an expanded disability status scale (EDSS). Neurology 1983;33:1444–1452.
21. Hirsch S, Klatt D, Freimann F, Scheel M, Braun J, Sack I. In vivo measurement of volumetric strain in the human brain induced by arterial pulsation and harmonic waves. Magn Reson Med 2012;70:671–683.
22. Rump J, Klatt D, Braun J, Warmuth C, Sack I. Fractional encoding of harmonic motions in MR elastography. Magn Reson Med 2007;57: 388–395.
23. Streitberger K-J, Reiss-Zimmermann M, Freimann FB, et al. High-resolution mechanical imaging of glioblastoma by multifrequency magnetic resonance elastography. PLoS One 2014;9:e110588.
24. Papazoglou S, Xu C, Hamhaber U, et al. Scatter-based magnetic resonance elastography. Phys Med Biol 2009;54:2229–2241.
25. Fehlner A, Papazoglou S, McGarry MD, et al. Cerebral multifrequency MR elastography by remote excitation of intracranial shear waves. NMR Biomed 2015;28:1426–1432.
26. Sack I. Magnetic resonance elastography 2.0: High resolution imaging of soft tissue elasticity, viscosity and pressure. Dtsch Med Wochenschr 2013;138:2426–2430.
27. Manduca A, Oliphant TE, Dresner MA, et al. Magnetic resonance elastography: non-invasive mapping of tissue elasticity. Med Image Anal 2001;5:237–254.
28. Ghiglia DC, Pritt MD. Two-dimensional phase unwrapping: theory, algorithms, and software. New York: John Wiley & Sons; 1998.
29. Sack I, Beierbach B, Wuerfel J, et al. The impact of aging and gender on brain viscoelasticity. Neuroimage 2009;46:652–657.
30. Tubridy N, Ader H, Barkhof F, Thompson A, Miller D. Exploratory treatment trials in multiple sclerosis using MRI. J Neurol Neurosurg Psychiatry 1998;64:50–55.
31. Avants BB, Tustison NJ, Song G, Cook PA, Klein A, Gee JC. A reproducible evaluation of ANTs similarity metric performance in brain image registration. Neuroimage 2011;54:2033–2044.
32. Sack I, Joehrens K, Wuerfel J, Braun J. Structure sensitive elastography: on the viscoelastic powerlaw behavior of in vivo human tissue in health and disease. Soft Matter 2013;9:5672–5680.
33. Muhlau M, Buck D, Forschler A, et al. White-matter lesions drive deep gray-matter atrophy in early multiple sclerosis: support from structural MRI. Mult Scler 2013;19:1485–1492.

34. Perez-Miralles F, Sastre-Garriga J, Tintore M, et al. Clinical impact of early brain atrophy in clinically isolated syndromes. Mult Scler 2013;19:1878–1886.

35. Barkhof F. The clinico-radiological paradox in multiple sclerosis revisited. Curr Opin Neurol 2002;15:239–245.

36. Johnson CL, McGarry MD, Gharibans AA, et al. Local mechanical properties of white matter structures in the human brain. Neuroimage 2013;79:145–152.

37. Murphy MC, Huston J 3rd, Jack CR Jr, et al. Measuring the characteristic topography of brain stiffness with magnetic resonance elastography. PLoS One 2013;8:e81668.

38. McGarry MDJ, Johnson CL, Sutton BP, et al. Suitability of poroelastic and viscoelastic mechanical models for high and low frequency MR elastography. Med Phys 2015;42:947–957.

39. Qin EC, Sinkus R, Geng G, et al. Combining MR elastography and diffusion tensor imaging for the assessment of anisotropic mechanical properties: a phantom study. J Magn Reson Imaging 2013;37:217–226.

40. Romano A, Scheel M, Hirsch S, Braun J, Sack I. In vivo waveguide elastography of white matter tracts in the human brain. Magn Reson Med 2012;68:1410–1422.